II. MATERIALS, METHODS, AND TECHNIQUES

A. Dispersion of gold nanoparticles in lyotropic LCs

GNRs of various sizes were examined. Comparatively large, polymer coated GNRs (Nanopartz Inc.) with a mean diameter of 40 nm and mean length of 73 nm are used as supplied. Smaller GNRs with a mean diameter of 20 nm and mean length of 50 nm were synthesized according to Ref. [29]. Gold nanocubes and gold "nanostars" were synthesized according to Refs. [30,31], respectively. Gold nanoparticles are functionalized by thiol-terminated methoxy-poly(ethylene glycol) (mPEG-SH) for colloidal stability. The composite of mPEG-GNRs and lyotropic LC is prepared based on a ternary lyotropic LC of sodium decyl sulfate-decanol-water (SDS–1-decanol–water) with a known phase diagram [32]. A calamitic nematic (N_C) lyotropic LC was prepared using a composition of 37.5 wt% of SDS, 5.5 wt% of 1-decanol (both

FIG. 2. (Color online) (a) SEM image of gold nanocubes. (b) Optical microscopy image of a dispersion of gold naoncubes in 5CB. The inset shows a vial with the gold nanocubes-5CB dispersion. (c) Polarization-independent extinction spectrum of gold nanocubes in 5CB. (d)

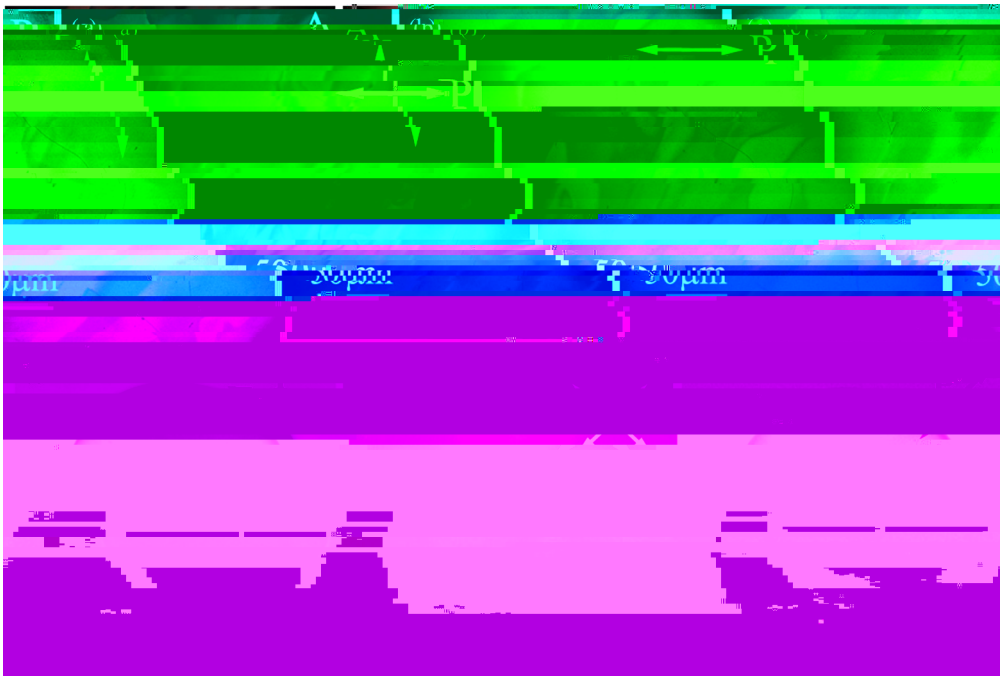

FIG. 3. (Color online) (a) POM image of a planar aligned 5CB sample between crossed polarizers. (b, c) Transmission mode AFM height and phase images of the 5CB sample in (a). (d) POM image of 5CB filled between crossed polarizers with PDMS rods. (e, f) Transmission mode AFM height and phase images of the 5CB sample in (d) showing the director field.

N (r) for N_C, as

5). Phase

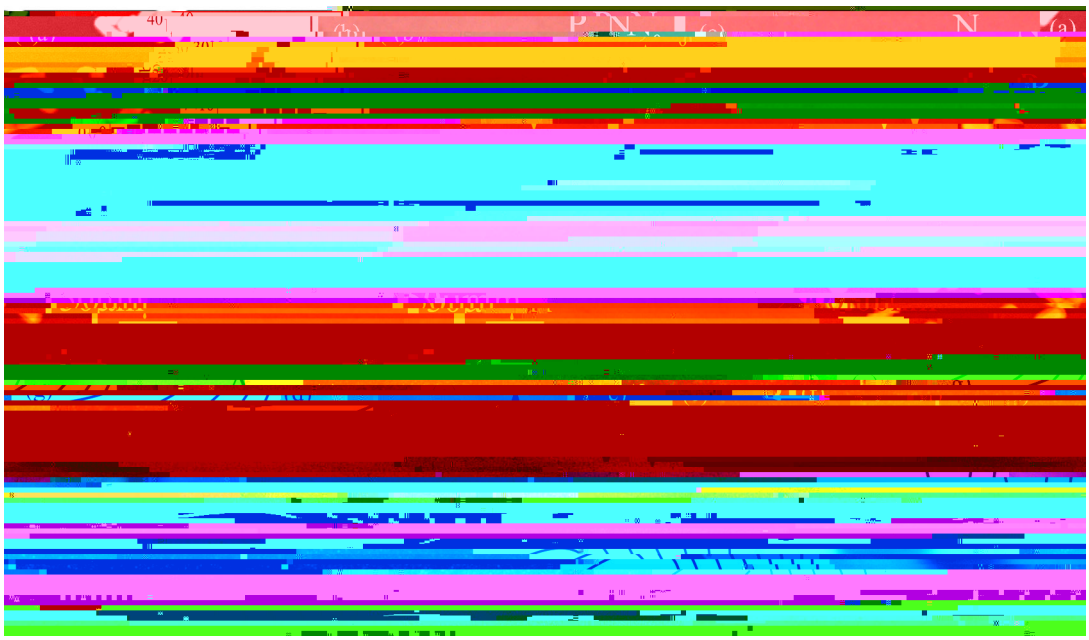

FIG. 4. (Color online) (a) SEM image of PDMS rods. The inset of (a) shows the cross section of the rods. (b, c) Transmission mode AFM height and phase images of the PDMS rods in (a). (d) POM image of 5CB filled between crossed polarizers with N_0. (e, f) Transmission mode AFM height and phase images of the 5CB sample in (d) showing the director field. (g) Azimuthal angle (ϕ) profile of the director field in (e). N_C (b) and

N (r) in (e).

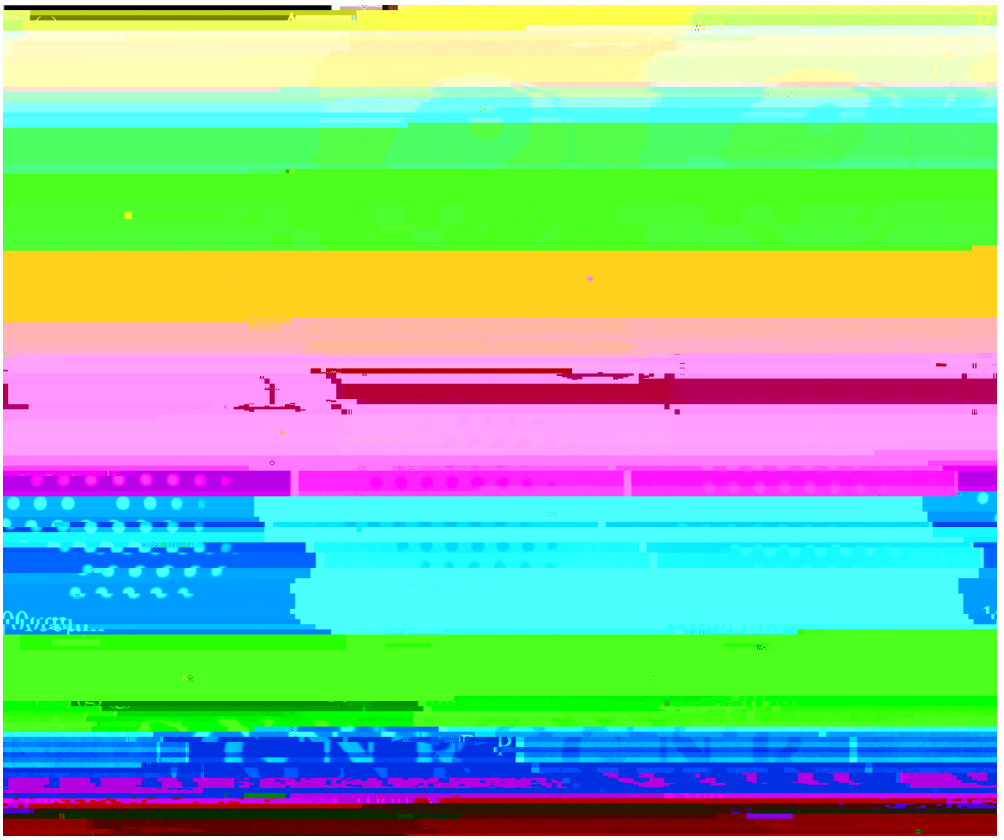

FIG. 5. (Color online) (a) A POM image of a typical bidisperse planar sample of 5CB

FIG. 6. (Color online) (a) A schematic of the setup used to measure the polarization-dependent transmitted spectra; the arrow indicates orientation of $\mathbf{N}_0$ set by the shear force. (b) Experimental extinction spectra of GNRs at 4.7×10^{-8} M. (c) Simulated extinction coefficients for the same concentration of GNRs as (b) for two orthogonal polarizations of incident light and $S_{GNR} = 1$. (d) Computer-simulated spectral dependencies of extinction, absorption, and scattering coefficients for two orthogonal polarizations of incident light for $S_{GNR} = 0.71$. (e) Calculated imaginary parts of refractive indices and its anisotropy. (f) Calculated spectral dependence of effective-medium refractive indices $n_{\parallel}$ and $n_{\perp}$.

at much lower concentrations or volume fractions of large GNRs. Third, the relative contribution of scattering to the total extinction ($\sigma_{abs}/\sigma_{ext}$) increases with increasing the effective volume of GNRs. For example, this ratio of GNRs of 20 nm in diameter and 50-nm long is 12%, while it increases to 52% for GNRs of 40 nm in diameter and 73 nm in length. This property makes dispersions of large GNRs good candidates for applications based on light scattering.

The quality of orientational ordering of GNRs in LC can be characterized by the scalar order parameter defined as

the absorption coefficient $\alpha_{\perp,\parallel}^{abs}$ in Fig. 6(d): $n_{\perp,\parallel}(\lambda) = n_{\perp,\parallel}^{offset} + [1/(2\pi^2)]\,P.V.\int_{\lambda_1}^{\lambda_2} \alpha_{\perp,\parallel}^{abs}(\lambda')/[1-(\lambda/\lambda')^2]\,d\lambda'$, where P.V. is the Cauchy principal value of the integral. The integration ranges from $\lambda_1 = 450$ nm to $\lambda_2 = 900$ nm. The used values of offset extraordinary and ordinary indices $n_{\perp,\parallel}^{offset}$ are based on $\bar{n}_{LC} = 1.39$ and the intrinsic optical anisotropy $\Delta n_{LC} = 0.006 \pm 0.001$ of the NC. The effective-medium optical anisotropy of the GNR-NC composite is much larger than the intrinsic birefringence of NC and changes sign at around the longitudinal SPR peak wavelength [Fig. 6(f)].

IV. DISCUSSION

A. Strong anchoring and elastic alignment

In general, the alignment of rod-like or other nonspherical particles dispersed in the nematic LC could be caused by GNR-LC matrix interaction in "strong," "weak," or finite surface anchoring regimes. In the strong anchoring regime, the GNR-matrix interaction is expected to be mediated mostly by the minimization of elastic free energy due to director distortions induced by nanoparticles while having the director at LC-GNR surfaces follow the tangential boundary conditions [21]. In contrast, in the regime of weak surface anchoring, the director distortions in the LC bulk and energetic cost due to them can be neglected as the director meets the GNR-LC surface at different angles, so that the anisotropic nanoparticle orientation is determined by minimization of the

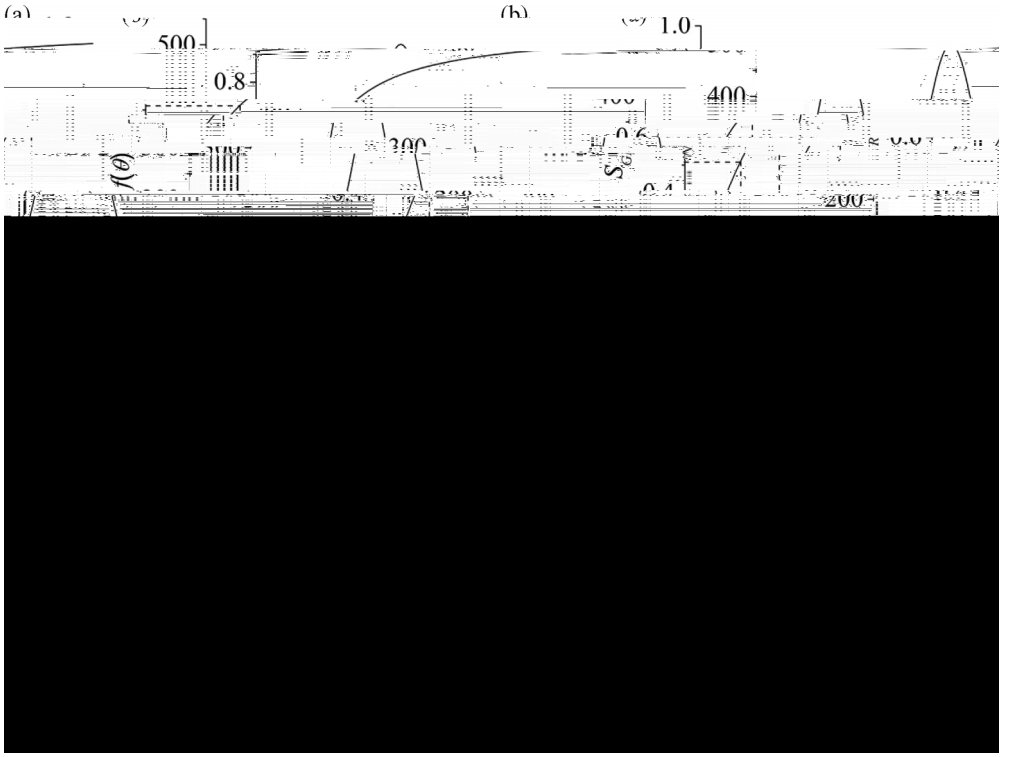

FIG. 7. (a) Orientation distribution function $f(\theta)$ versus θ for different S_G values at $\kappa = LRW/(k_BT)$. (b) Nematic order parameter S_G versus κ for different r_f values. (c) Effective SPR versus r_f at $S_G = 0.71$. (d) Order parameter S_G versus r_f.

is a function of the angle between the fiber axis and the director. The orientation distribution function for each fiber orientation is assumed to be the same. Therefore, the orientation distribution function $f_s(\theta)$ per unit area ($\sin\theta\, d\theta$), versus $\kappa = LRW/(k_BT)$. The nematic order parameter S_G is defined as

$$S_G = \int_0^{\pi} P_2(\cos\theta) f_s(\theta) \sin\theta\, d\theta = 3\pi(\quad)[2 \quad f(i \quad/i)]$$

V. CONCLUSION

[39] P. K. Jain, K. S. Lee, I. H. El-Sayed, and M. A. El-Sayed, J. Phys. Chem. B 110, 7238 (2006).
[40] E. D. Palik, Handbook of Optical Constants of Solids (Academic, New York, 1998).
[41] M. F. Islam, D. E. Milkie, C. L. Kane, A. G. Yodh, and J. M. Kikkawa, Phys. Rev. Lett. 93, 037404 (2004).
[42] E. Charlet and E. Grelet, Phys. Rev. E 78, 041707 (2008).
[43] C. J. Smith and C. Dennison, J. Appl. Phys. 101, 014305 (2007).
[44] A. V. A. Pinto and L. Q. Amaral, J. Phys. Chem. 94, 3186 (1990).
[45] P.-G. de Gennes and J. Prost, The Physics of Liquid Crystals (Clarendon, Oxford, 1995).
[46] P. van der Schoot, V. Popa-Nita, and S. Kralj, J. Phys. Chem. B 112, 4512 (2008).
[47] A. M. Ribas, L. R. Evangelista, A. J. Palangana, and E. A. Oliveira, Phys. Rev. E 51, R5204 (1995).